Eur. Phys. J. Plus (2018) **133**: 10
DOI 10.1140/epjp/i2018-11837-y

THE EUROPEAN PHYSICAL JOURNAL PLUS

Regular Article

Effect of the end sill angle on the hydrodynamic parameters of a stilling basin

Faezeh Tajabadi[1], Ehsan Jabbari[1], and Hamed Sarkardeh[2,a]

[1] Department of Civil Engineering, University of Qom, Qom, Iran
[2] Department of Civil Engineering, Faculty of Engineering, Hakim Sabzevari University, Sabzevar, Iran

Received: 14 May 2017 / Revised: 6 December 2017
Published online: 16 January 2018 –

Abstract. In this study, the effect of an end sill angle on the hydrodynamic parameters of a stilling basin, such as pressure, velocity, turbulence intensity, vorticity and energy dissipation, is investigated numerically. Simulations are performed using RNG and VOF for turbulence and free surface models, respectively. After verifying the numerical results with the experimental data, the effect of four end sill angles of 30°, 45°, 60° and 90° on the flow parameters in the stilling basin is analyzed. Results show that the stilling basin with triangle end sill with angle of 60° has the best performance by dissipating 62% of energy.

1 Introduction

In high dams, stilling basins are employed to dissipate the extra energy of flow and protect the downstream against scouring and erosion. Formation of hydraulic jumps in the stilling basin is a mechanism to dissipate energy. Using blocks and sills with different geometries and arrangements increases the performance of stilling basin in dissipating energy and consequently reduces the length of the basin. Hager and Li [1] classified different formed jumps over a vertical sill (fig. 1).

As can be seen from fig. 1, the maximum sequent depth ratio occurs in the A-jump, and the sill has no effect on the jump (fig. 1(a)). The B-jump occurs when the tailwater depth decreases and consequently the toe of the jump moves toward the sill and the streamline pattern becomes curved over the sill (fig. 1(b)). The minimum B-jump is the formation of a second roller at the downstream of the sill zone and a C-jump forms when the maximum difference between the depth of the flow over the sill and the tailwater depth occurs (figs. 1(c) and (d)). By decreasing the tailwater depth and increasing the disturbance of the flow, the D-jump forms and scouring is expectable (fig. 1(e)) [1].

In the recent years, many researches were performed to study the behaviour of the flow in stilling basins in different conditions. Mardani *et al.* [2] analyzed the effect of installing blocks on the performance of stilling basins in different block arrangements and hydraulic conditions, experimentally. Debabeche and Achour studied the effect of a continuous sill on the hydraulic jump in a triangle channel [3]. Deng *et al.* presented the prototype measurements of pressure fluctuations for a hydraulic jump and estimated the incident velocity to the end sill [4]. Yan *et al.* performed a statistical analysis of pressure fluctuations at the bottom of spatial hydraulic jumps with abrupt lateral expansions. Tajabadi *et al.* [5] studied the effect of using different end sill angles and standard USBR type on hydrodynamic parameters of the flow in the stilling basin, numerically. Tokyay *et al.* [6] and Altan-Sakarya and Tokyay [7] performed a numerical simulation of A- and B-jumps in a positive step and horizontal rectangular channels having an abrupt drop. Alikhani *et al.* carried out experiments to evaluate the effects of a single vertical continuous sill and its position on control of depth and length of a forced jump in a stilling basin without considering tailwater depth, which is variable and totally controlled by downstream river conditions [8]. Behrouzi-Rad *et al.* performed experiments on a series of perforated sills with different heights and ratio. Their results confirmed the significant effect of the perforated sill on the dissipation of energy and reduction of the length of the basin [9]. Carvalho *et al.* based on a two-dimensional (2D) numerical model and a re-normalisation group (RNG) k-ε for turbulence modeling, stated that Reynolds averaged Navier-Stockes (RANS) equations are appropriate for hydraulic jump problems and the agreement between the numerical results and laboratory measurements was satisfactory [10]. Kazemi *et al.* [11] represented the experimental measurements of pressure fluctuations in stilling basin. Naseri *et al.* [12] numerically simulated pressure fluctuations in the stilling basins

[a] e-mail: sarkardeh@hsu.ac.ir

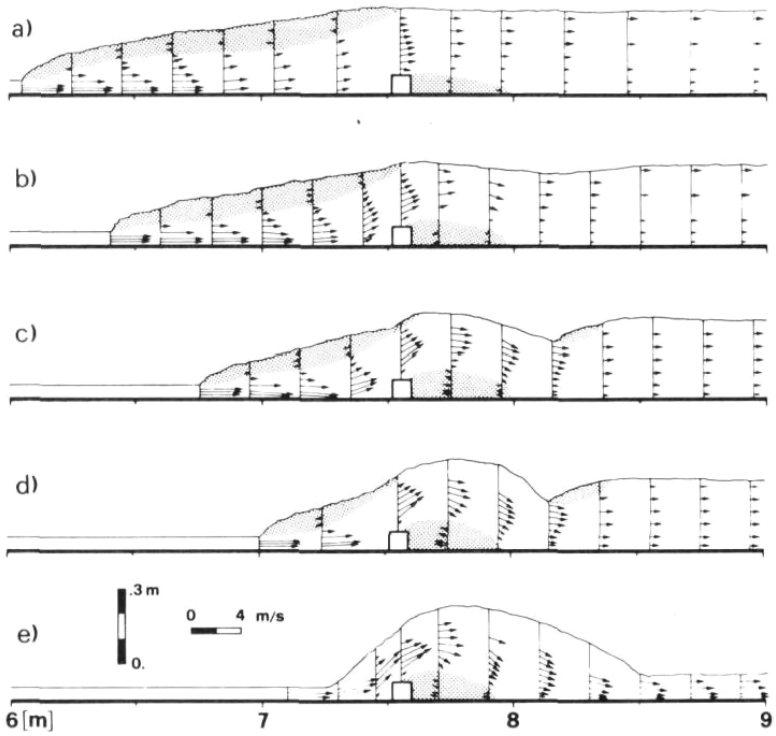

Fig. 1. Controlling flow using a vertical sill. Taken from [1].

with different inlet flow conditions using the volume of fluid (VOF) and large eddy simulation (LES) models for free surface and turbulence. Liu *et al.* presented the results of a laboratory study on the turbulence structure of hydraulic jumps with low Froude number (Fr) [13]. Zobeyer *et al.* investigated turbulence characteristics of the transition region from hydraulic jump to open channel flow [14]. Valero *et al.* carried out numerical investigation of USBR type III stilling basin performance at different Fr and showed that, when a stepped chute is considered, the flow is continuously fed with turbulence throughout the spillway chute, and the turbulence generated via impingement is smaller than for a smooth chute [15]. Traditionally, physical models were used as a safe way to analyze the flow through or over the hydraulic structures [16–22]. However, today, using numerical simulations along with the experimental data is the cheapest method to solve complex problems in hydraulic engineering [23–29].

Although many studies have been carried out on flow parameters in stilling basins with different conditions, few attempts have been made to numerically simulate the end sill geometry and its effect on the flow behavior in the basin. The aim of this study is to show the effect of the end sill angle on the hydrodynamic parameters of stilling basins. After validation of the numerical model, pressure, velocity, vorticity, turbulence intensity and energy dissipation in the presence of four different end sill angles were compared and analyzed.

2 Materials and methods

RANS equations of fluid motion in 3D form were solved based on the finite volume method (FVM) using the `Flow 3D` software. For simulating the rigid surfaces, the fractional area-volume obstacle representation (FAVOR) was employed. The VOF method also was used to track the free surface [30]. The general governing RANS and continuity equations for incompressible fluid, including the VOF and FAVOR variables, are the following:

$$\partial(uA_x)/\partial x + \partial(vA_y)/\partial y + \partial(wA_z)/\partial z = 0, \tag{1}$$

$$\partial u_i/\partial t + (1/V_F)(u_i A_i \partial u_i/\partial x_i) = (1/\rho)(\partial P/\partial x_i) + g_i + f_i, \tag{2}$$

in which u, v and w represent the velocities in the x-, y- and z-direction, respectively, V_F is the volume fraction of the fluid in each cell, A_x, A_y and A_z are the fractional areas open to the flow in the x-, y- and z-direction, respectively, ρ is the density, i shows the coordinates direction (*i.e.* x, y, and z), P is defined as the pressure, g_i is the gravitational force in the subscript direction and f_i represents the Reynolds stresses for which a turbulence model is required for closure. In order to verify the numerical model, the experimental data of the Khodafarin stilling basin model was used. Plan and longitudinal section of the stilling basin are shown in fig. 2 [31].

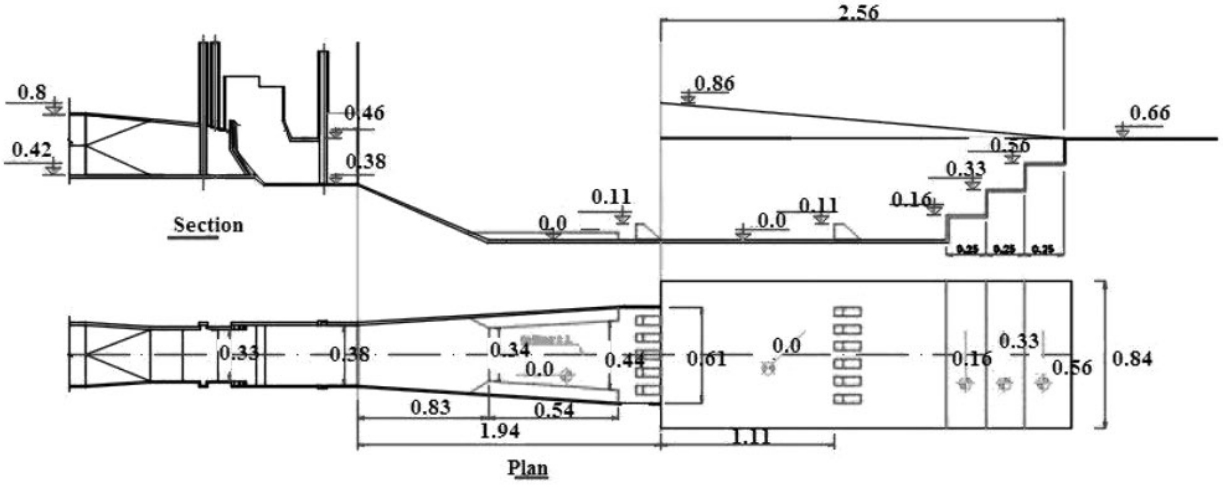

Fig. 2. Plan and longitudinal section of the Khodafarin stilling basin. Taken from [31].

Fig. 3. Physical model of stilling basin. Taken from [31].

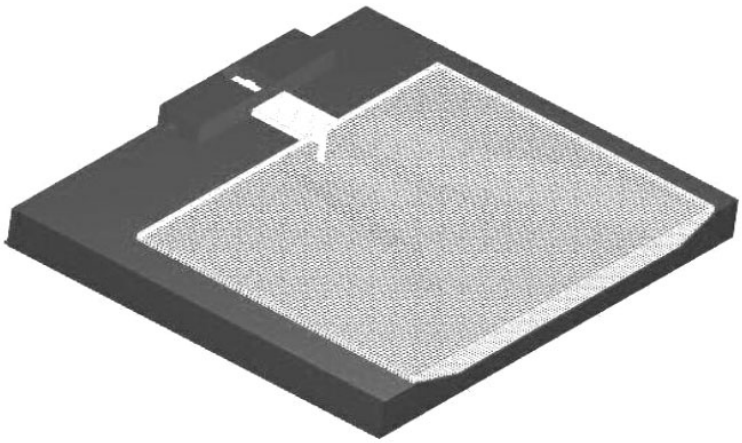

Fig. 4. Mesh blocks in the numerical model.

The first part of the stilling basin has a length of 0.83 m and 1V:2H. Then a basin with horizontal bed with a length of 3.71 m is located where two rows of blocks and a stepped end sill are located on it. All the components of the basin are made of plexiglass and blocks are made of wood. The physical model of the stilling basin is shown in fig. 3 [31].

In order to study convergence and accuracy of the numerical model, two different mesh blocks with different cell sizes were selected (fig. 4).

Table 1. Boundary conditions in the numerical model.

Boundaries	$X_{\min}$	$X_{\max}$	$Y_{\min\,,\max}$	$Z_{\min}$	$Z_{\max}$
Block 1	Volume Flow Rate	Continuative	Wall	Wall	Symmetric
Block 2	Continuative	Specified Pressure	Wall	Wall	Symmetric

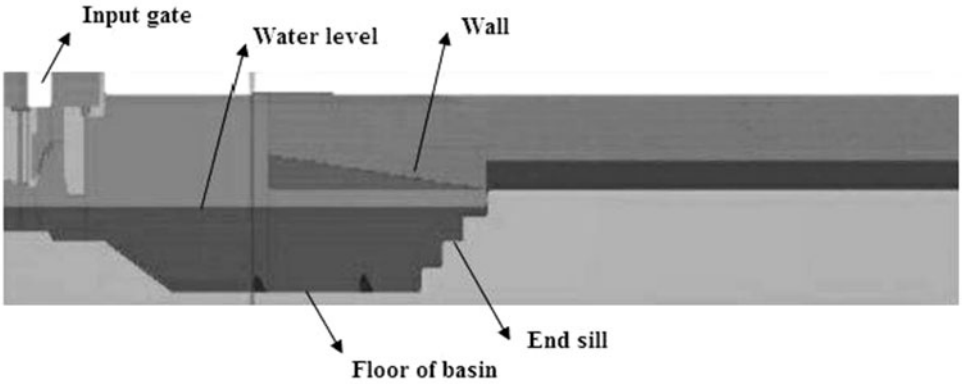

Fig. 5. Initial conditions imposed on the numerical model.

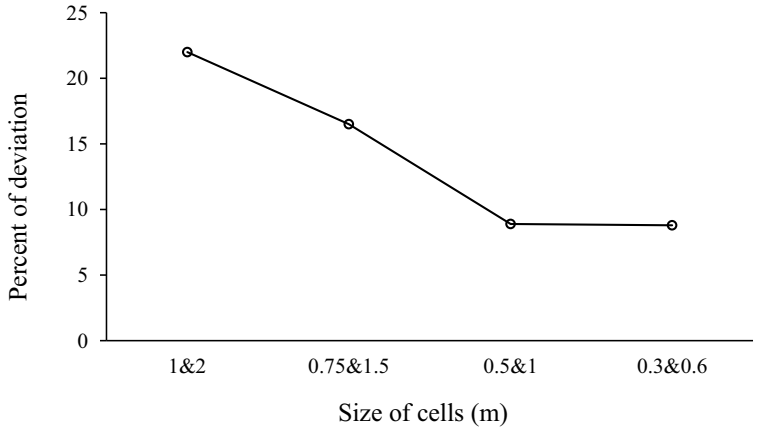

Fig. 6. Sensitivity analysis of the mesh size in the numerical model.

Table 1 shows the defined boundary conditions of the numerical model. At the inlet of the mesh block 1, the volume flow rate (with $Q = 0.546\,\mathrm{m}^3/\mathrm{s}$ in the physical model) was considered, and, for the outlet of the mesh block 2, the specified pressure (with $H = 0.17\,\mathrm{m}$ in the physical model) was considered. To simulate the atmospheric pressure on the top surface of the mesh blocks, the symmetric boundary condition was employed. Moreover, the wall boundary condition in form of no-slip was selected for the bottom and sides. For possibility of comparison between hydrodynamic parameters, all cases after verification were simulated in the same Fr equal to 3.56.

As the initial condition, the hydrostatic pressure in the z-direction and water as an incompressible fluid with density $1000\,\mathrm{kg/m}^3$ and dynamic viscosity $0.001\,\mathrm{kg/m/s}$ at $20\,^\circ\mathrm{C}$ were defined, to reduce the time of calculation and provide a faster stability in the numerical model (fig. 5).

In order to obtain the optimum size of cells, the sensitivity analysis was carried out for four different sizes of cells in both blocks as 1-2, 0.75-1.5, 0.5-1 and 0.3-0.6, in which the first and the second number are the size of cubic cells for the first and second blocks, respectively.

As can be seen from fig. 6, the percent of deviation represents the difference between the measured values in numerical and physical models for the velocity parameter in the tail water, which shows cells with size of 0.3-0.6 have acceptable results, and therefore it was selected. As for previous researches, the RNG turbulence model combined with the VOF method has a good performance in simulating the stilling basin [32–34]. Therefore, the RNG turbulence model was selected in this study.

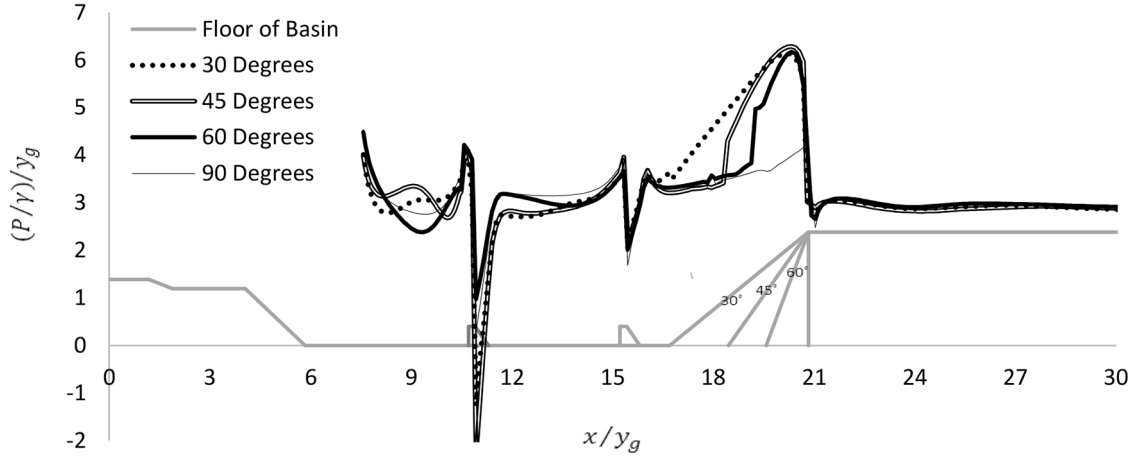

Fig. 7. Dimensionless pressure profiles in different end sill angles.

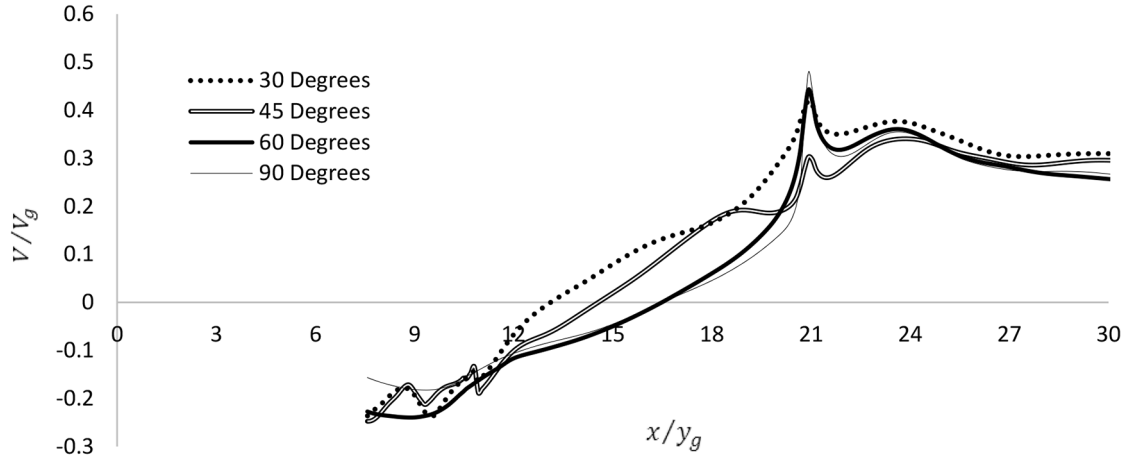

Fig. 8. Dimensionless velocity profiles in different end sill angles.

3 Results and discussions

In this research, hydrodynamic parameters, such as pressure, velocity, turbulence intensity, vorticity and energy dissipation, were numerically calculated and analyzed for understanding the flow behavior in the stilling basin with different end sill geometries. Figure 7 shows dimensionless pressure profiles for stilling basins with a triangle end sill with different angles including 30, 45, 60 and 90 degrees.

As is clear from fig. 7, where y_g is the jet thickness below the gate at full opening condition (0.28 m in the physical model) and γ is the specific gravity of water, blocks and end sills with different angles cause the velocity to be reduced and the pressure to be increased in the basin. Changes in the end sill angle have modified the pressure profile, in particular over the end sill. At the location of the end sill, the pressure in the stilling basin with end sill angles of 30°, 45° and 60° compared with that of 90° was increased by about 33%, 32% and 29%, respectively. Moreover, looking at fig. 7, changing the angle of the end sill has little effect on the pressure at the downstream of the end sill, while pressure reduces significantly and becomes constant. Dimensionless velocity profiles for four different end sill angles are shown in fig. 8 where V_g is the flow velocity below the gate at full opening and is equal to 5.8 m/s in the physical model.

As can be seen from fig. 8, in all cases, due to the presence of return flow and vortices, the velocity at the beginning of the basin is negative. The effect of the end sill with an angle of 60° compared with that of 90°, 45° and 30° on the decreasing velocity of the flow is greater by about 4%, 13% and 17%, respectively. Also, the flow velocity at the downstream of the end sills decreases due to the increase in the pressure. Regarding the definition of turbulence intensity (I) [30], this parameter was analyzed at different end sill angles in fig. 9.

According to fig. 9, at the beginning of the stilling basin, in all cases, due to formation of hydraulic jump and return flows, turbulence intensity is high and near the end of the basin, it decreases and, finally, in the tail water becomes constant. In fig. 10, the vorticity parameter (W_y) [30] in the y-direction (xz-plane and during the longitudinal axis of the basin) is analyzed.

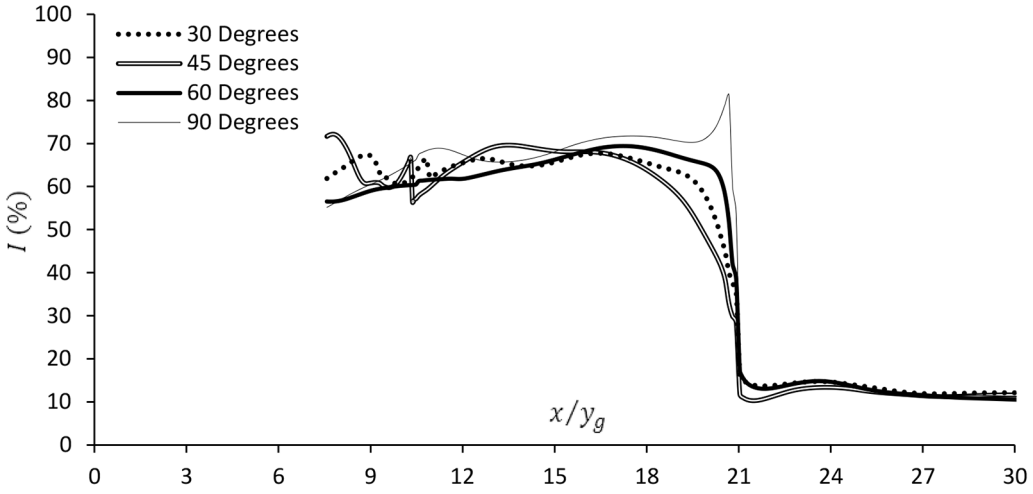

Fig. 9. Turbulence intensity profiles for four stilling basins.

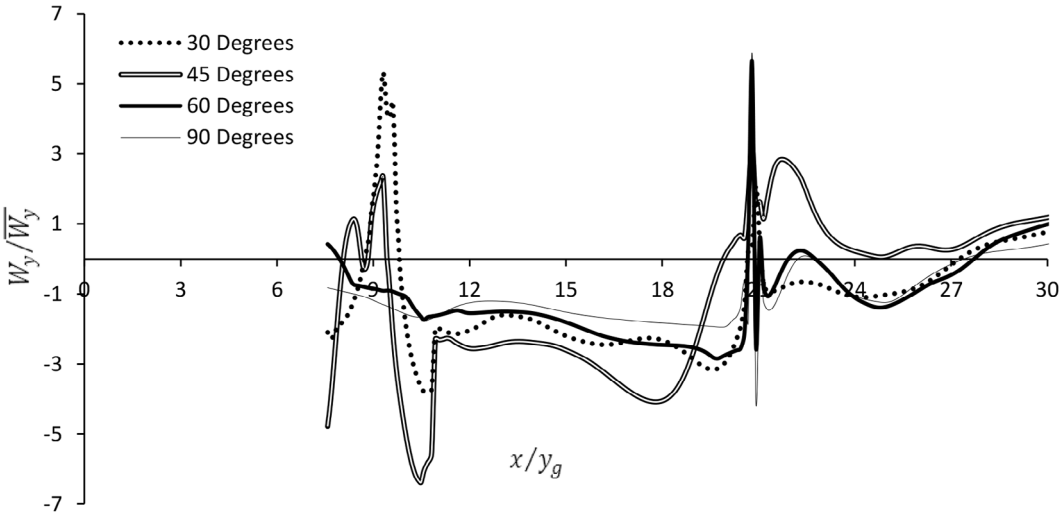

Fig. 10. Vorticity in y-direction at different end sill angles.

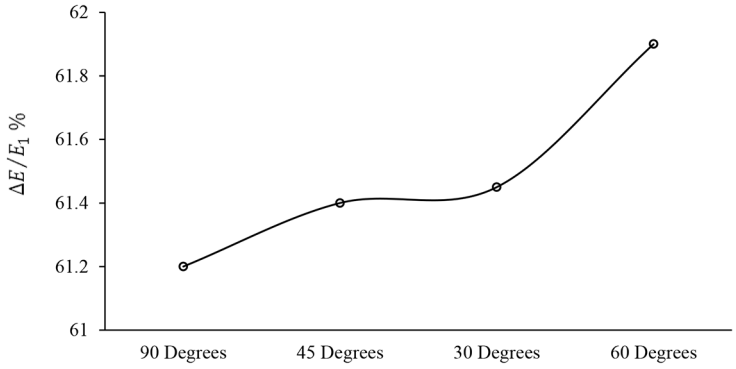

Fig. 11. Energy dissipation ratio in different end sill angles.

Figure 10 shows that the vorticity parameter in the y-direction is negative in all cases (because the amount of vorticity increases and the rotating direction changes due to the impact of the flow with blocks and end sill). In general, the end sill with an angle of 60° causes more reduction of vorticity, around the y-direction, compared with the end sills with angles of 45°, 30° and 90° by about 3.5%, 30% and 90%, respectively. Figure 11 shows the energy dissipation ratio at different end sill angles, where $\Delta E = E_1 - E_2, E_1 = V_1^2/2g + P_1/\gamma$, $E_2 = V_2^2/2g + P_2/\gamma$.

As can be seen from fig. 11, the effect of the end sill angle the on energy dissipation ratio is not considerable; however, an end sill with an angle of 60° has better performance compared to other angles.

4 Conclusions

In this numerical study, the effect of the end sill angle at the end of a stilling basin on the hydrodynamic parameters, such as pressure, velocity, turbulence intensity, vorticity and energy dissipation, was studied. Simulations were performed by employing RNG and VOF as the turbulence and free surface models. After verifying the numerical model with the experimental data, four different end sill angles, including 30°, 45°, 60° and 90°, were simulated and analyzed. Results show that at the location of the end sill, pressure increases in the stilling basin with end sill angles of 30°, 45° and 60° compared with that of 90° by about 33%, 32% and 29%, respectively. The effect of the end sill with angle of 60° compared with the end sill with angles of 90°, 45° and 30° on decreasing velocity of the flow was more about 4%, 13% and 17%, respectively. At the beginning of the stilling basin, in all cases, due to the formation of hydraulic jump and return flows, the turbulence intensity is high and near the end of the basin, the turbulence intensity decreases and, in the tail, water becomes constant. In general, the end sill with angle of 60° causes a greater reduction of vorticity around the y-direction, compared with end sills with angles of 45°, 30° and 90°, by about 3.5%, 30% and 90%, respectively. Finally, it was found that the effect of the end sill angle on the dissipating energy of the flow is not considerable.

The authors would like to thank the Hydraulic Structures Division of the Water Research Institute for their kind cooperation in using experimental data.

References

1. W.H. Hager, D. Li, J. Hydraul. Res. **30**, 165 (1992).
2. M. Mardani, H. Rahimzadeh, H. Sarkardeh, Modares Mech. Eng. **15**, 31 (2015) (in Persian).
3. M. Debaaeche, B. Achour, J. Hydraul. Res. **45**, 135 (2007).
4. Z. Deng, G.R. Guensch, M.C. Richmond, M.A. Weiland, T.J. Carson, J. Hydraul. Res. **45**, 674 (2007).
5. F. Tajabadi, E. Jabbari, H. Sarkardeh, Iran. Dam Hydroelectr. Powerplant **4**, 43 (2017) (in Persian).
6. N.D. Tokyay, A.B. Altan-Sakarya, E. Eski, Int. J. Numer. Methods Fluids **56**, 1605 (2006).
7. A.B. Altan-Sakarya, N.D. Tokay, Can. J. Civ. Eng. **27**, 805 (2000).
8. A. Alikhani, R. Behrozi-Rad, M. Fathi-Moghadam, Int. J. Phys. Sci. **5**, 25 (2010).
9. R. Behrouzi-Rad, M. Fathi-Moghadam, H.R. Ghafouri, A. Alikhani, Wulfenia J. **20**, 300 (2013).
10. R.F. Carvalho, C.M. Lemos, C.M. Ramos, J. Hydraul. Res. **46**, 739 (2008).
11. F. Kazemi, S.R. Khodashenas, H. Sarkardeh, Int. J. Civ. Eng. **14**, 13 (2016).
12. F. Naseri, H. Sarkardeh, E. Jabbari, Acta Mech. (2017) https://doi.org/10.1007/s00707-017-2069-z.
13. M. Liu, N. Rajaratnam, D. Zhu, J. Hydraul. Eng. ASCE **130**, 511 (2004).
14. H. Zobeyer, N. Jahan, Z. Islam, N. Rajaratnam, J. Hydraul. Res. **48**, 395 (2014).
15. D. Valero, D. Bung, B. Crookston, J. Matos, *Numerical investigation of USBR type III stilling basin performance downstream of smooth and stepped spillways*, in *Hydraulic Structures and Water System Management: 6th IAHR International Symposium on Hydraulic Structures*, edited by B. Crookston, B. Tullis (2016) pp. 652–663, http://doi.org/10.15142/T340628160853.
16. M. Monshizadeh, A. Tahershamsi, H. Rahimzadeh, H. Sarkardeh, Eur. Phys. J. Plus **132**, 329 (2017).
17. M. Azarpira, H. Sarkardeh, S. Tavakkol, R. Roshan, H. Bakhshi, Sadhana **39**, 1201 (2014).
18. O. Nazari, E. Jabbari, H. Sarkardeh, Int. J. Civ. Eng. **13**, 45 (2015).
19. M. Marosi, M. Ghomeshi, H. Sarkardeh, Sadhana **40**, 1373 (2015).
20. H. Sarkardeh, A.R. Zarrati, E. Jabbari, M. Marosi, Eng. Appl. Comput. Fluid Mech. **8**, 598 (2014).
21. H. Sarkardeh, M. Marosi, R. Roshan, Int. J. Energy Environ. **6**, 597 (2015).
22. R. Roshan, H. Sarkardeh, A.R. Zarrati, *Vortex study on a hydraulic model of Godar-e-Landar Dam and hydropower plant*, in *Computational Methods in Multiphase Flow V*, edited by A. Mammoli, *WIT Transactions on Engineering Sciences*, Vol. **63** (WIT Press, 2009) pp. 217–225, https://doi.org/10.2495/MPF090191.
23. S.A.H. Sajjadi, S.H. Sajjadi, H. Sarkardeh, Int. J. Civ. Eng. (2016) https://doi.org/10.1007/s40999-016-0113-3.
24. H. Sarkardeh, E. Jabbari, A.R. Zarrati, S. Tavakkol, Proc. Inst. Civ. Eng. Water Manage. **167**, 356 (2014).
25. R. Maghsoodi, M.S. Roozgar, H. Sarkardeh, H.M. Azamathulla, Int. J. Model. Simul. **32**, 237 (2012).
26. H. Rahimzadeh, R. Maghsoodi, H. Sarkardeh, S. Tavakkol, Eng. Appl. Comput. Fluid Mech. **6**, 100 (2012).
27. M. Jorabloo, R. Maghsoodi, H. Sarkardeh, J. Am. Sci. **7**, 931 (2011).
28. R. Maghsoodi, M.S. Roozgar, K.W. Chau, H. Sarkardeh, J. Dam Eng. **2**, 1 (2012).
29. H. Sarkardeh, Meccanica **52**, 3629 (2017).
30. Flow Science, Inc. (2012). Flow 3D Documentation, Release 10.1.0.
31. Water Research Institute (WRI), *Physical Model Study of Khodaafarin Dam*, Technical Report (2015).
32. S.R. Sabbagh-Yazdi, F. Rostami, in *12th WSEAS International Conference Applied Mathematics, Cairo* (WSEAS, 2007) pp. 168–174.
33. H.R. Babaaali, A. Shamsai, H.R. Vosoghifar, Arab. J. Sci. Eng. **40**, 381 (2015).
34. A. Abbaspour, D. Farsadizadeh, A.H. Dalir, A.A. Sadraddini, J. Eng. Environ. Sci. **33**, 61 (2009).